

STAR FORMATIONS RATES AND STELLAR MASSES OF $Z = 7 - 8$ GALAXIES FROM IRAC OBSERVATIONS OF THE WFC3/IR ERS AND THE HUDF FIELDS¹

I. LABBÉ^{2,3}, V. GONZÁLEZ⁴, R. J. BOUWENS^{4,5}, G. D. ILLINGWORTH⁴, M. FRANX⁵, M. TRENTI⁶, P. A. OESCH⁷, P. G. VAN DOKKUM⁸, M. STIAVELLI⁹, C. M. CAROLLO⁷, M. KRIEK¹⁰, D. MAGEE⁴

Draft version October 31, 2018

ABSTRACT

We investigate the Spitzer/IRAC properties of 36 $z \sim 7$ z_{850} -dropout galaxies and 3 $z \sim 8$ Y_{098} galaxies derived from deep/wide-area WFC3/IR data of the Early Release Science, the ultra-deep HUDF09, and wide-area NICMOS data. We fit stellar population synthesis models to the SEDs to derive mean redshifts, stellar masses, and ages. The $z \sim 7$ galaxies are best characterized by substantial ages (> 100 Myr) and $M/L_V \approx 0.2$. The main trend with decreasing luminosity is that of bluing of the far- UV slope from $\beta \sim -2.0$ to $\beta \sim -3.0$. This can be explained by decreasing metallicity, except for the lowest luminosity galaxies ($0.1 L_{z=3}^*$), where low metallicity and smooth SFHs fail to match the blue far- UV and moderately red $H - [3.6]$ color. Such colors may require episodic SFHs with short periods of activity and quiescence (“on-off” cycles) and/or a contribution from emission lines. The stellar mass of our sample of $z \sim 7$ star forming galaxies correlates with SFR according to $\log M^* = 8.70(\pm 0.09) + 1.06(\pm 0.10) \log SFR$, implying star formation may have commenced at $z > 10$. No galaxies are found with SFRs much higher or lower than the past averaged SFR suggesting that the typical star formation timescales are probably a substantial fraction of the Hubble time. We report the first IRAC detection of Y_{098} -dropout galaxies at $z \sim 8$. The average rest-frame $U - V \approx 0.3$ (AB) of the 3 galaxies are similar to faint $z \sim 7$ galaxies, implying similar M/L . The stellar mass density to $M_{UV,AB} < -18$ is $\rho^*(z=8) = 1.8_{-1.0}^{+0.7} \times 10^6 M_\odot \text{Mpc}^{-3}$, following $\log \rho^*(z) = 10.6(\pm 0.6) - 4.4(\pm 0.7) \log(1+z) [M_\odot \text{Mpc}^{-3}]$ over $3 < z < 8$.

Subject headings: galaxies: evolution — galaxies: high-redshift

1. INTRODUCTION

Until recently, only a modest number of relatively bright $z \gtrsim 7$ galaxies were known, mostly from wide-area NICMOS (Bouwens et al. 2008; Oesch et al. 2009a, R. J. Bouwens et al. in preparation) and ground-based searches (Ouchi et al. 2009; Castellano et al. 2009; Hickey et al. 2009). The arrival of WFC3/IR aboard

HST has dramatically improved the situation by identifying large numbers of $z \gtrsim 7$ galaxies by their redshifted UV light. Here we report on $z \gtrsim 7$ galaxies selected from the WFC3/IR Early Release Science (ERS) observations over the GOODS-South field (Wilkins et al. 2009, R. J. Bouwens et al. in preparation), complemented with candidates from the recent ultra-deep survey with WFC3/IR over the HUDF09 field (Oesch et al. 2010; Bouwens et al. 2010a; see also McLure et al. 2009; Bunker et al. 2009; Yan et al. 2009).

Little is known about the stellar masses, metal production, and the contribution of star formation to reionization in these galaxies. Mid-infrared observations with the InfraRed Array Camera (IRAC; Fazio et al. 2004) on *Spitzer* can be used to constrain the stellar masses and ages, which has led to the surprising discovery of quite massive $\sim 10^{10} M_\odot$ galaxies at $z \gtrsim 6$ (Eyles et al. 2005; Yan et al. 2006; Stark et al. 2009) and appreciable ages (200–300 Myr) and M/L s as early as $z \sim 7$ (Egami et al. 2005; Labbé et al. 2006; Gonzalez et al. 2009). The overall results suggest the galaxies formed substantial amounts of stars at even earlier times, well into the epoch of reionization (Stark et al. 2007; Yan et al. 2006; Labbé et al. 2010).

In this Letter, we study the stellar populations of the largest sample of $z \gtrsim 7$ galaxies with IRAC measurements to date, focusing on correlations with luminosity and stellar mass, and implications for the mass density and $z \sim 8$. We adopt an $\Omega_M = 0.3, \Omega_\Lambda = 0.7$ cosmology with $H_0 = 70 \text{ km s}^{-1} \text{Mpc}^{-1}$. Magnitudes are in the AB photometric system (Oke & Gunn 1983).

ivo@obs.carnegiescience.edu

¹ Based on observations made with the NASA/ESA Hubble Space Telescope, which is operated by the Association of Universities for Research in Astronomy, Inc., under NASA contract NAS 5-26555. These observations are associated with programs #11563, 9797. Based on observations with the *Spitzer Space Telescope*, which is operated by the Jet Propulsion Laboratory, California Institute of Technology under NASA contract 1407. Support for this work was provided by NASA through contract 125790 issued by JPL/Caltech. Based on service mode observations collected at the European Southern Observatory, Paranal, Chile (ESO Program 073.A-0764A). Based on data gathered with the 6.5 meter Magellan Telescopes located at Las Campanas Observatory, Chile.

² Carnegie Observatories, Pasadena, CA 91101

³ Hubble Fellow

⁴ UCO/Lick Observatory, University of California, Santa Cruz, CA 95064

⁵ Leiden Observatory, Leiden University, NL-2300 RA Leiden, Netherlands

⁶ University of Colorado, Center for Astrophysics and Space Astronomy, 389-UCB, Boulder, CO 80309, USA

⁷ Institute for Astronomy, ETH Zurich, 8092 Zurich, Switzerland

⁸ Department of Astronomy, Yale University, New Haven, CT 06520

⁹ Space Telescope Science Institute, Baltimore, MD 21218, United States

¹⁰ Department of Astrophysical Sciences, Princeton University, Princeton, NJ 08544

2. OBSERVATIONS AND STELLAR POPULATION MODELING

Our sample consists of sources derived from the ultra-deep WFC3/IR HUDF, the deep WFC3/IR ERS, and wide-area NICMOS over the CDF-S and CDF-N. Candidates were selected using the $z \sim 7$ z_{850} -dropouts and $z \sim 8$ Y_{098} -dropouts, as used in Oesch et al. (2010), Bouwens et al. (2010b), and Gonzalez et al. (2009) (see also R. J. Bouwens et al. in preparation). We now briefly discuss the IRAC photometry from the new ERS sample.

The Spitzer/IRAC data over the WFC3/ERS area in the CDF-S (≈ 23.3 hours integration time) was obtained from the Great Observatories Origins Deep Survey (GOODS; M. Dickinson et al. in preparation).¹¹ The IRAC depths in the 3.6 and 4.5- μ m bands are 27.1 and 26.5 magnitude (1σ , total, point source), respectively. Obtaining reliable IRAC fluxes of the candidates is challenging because of the contamination from the extended PSF wings of nearby foreground sources. We remove contaminating flux, by modeling the candidates and nearby sources using their isolated flux profiles and positions in the deep WFC3/IR maps as templates. We convolve the templates to match the IRAC PSF, simultaneously fit them to the IRAC map leaving only the fluxes as free parameters, and subtract the best-fit models to the foreground sources (see Labbé et al. 2006; Wuyts et al. 2007; Gonzalez et al. 2009; de Santis et al. 2007). After cleaning the IRAC images, we perform conventional aperture photometry in the 3.6 and 4.5 μ m bands in $2''.5$ diameter apertures on 15 of the original 18 z_{850} -dropout galaxies over the WFC3/IR ERS. Three were too close to bright sources for reliable measurement. Fluxes were corrected by a factor $\times 1.8$ to account for light outside the aperture (consistent with point source profiles). Six of the 15 galaxies are undetected in IRAC ($[3.6] < 26.5, 2\sigma$). Errors include the uncertainty in the best-fit confusion correction, added in quadrature.

We complete the sample with 21 $z \sim 7$ galaxies with IRAC measurements from the HUDF (Oesch et al. 2010; Labbé et al. 2010) and from the recent wide-area NICMOS search (Gonzalez et al. 2009, R. J. Bouwens, in preparation). The total sample consists of 36 $z \sim 7$ galaxies spanning 4 magnitudes in H_{160} . To investigate trends with magnitude, we stacked the flux densities of the galaxies in three ~ 1 -magnitude bins centered on $H_{160} \approx 26, 27$ and 28 , containing 11, 15, and 10 galaxies respectively. The uncertainties are determined by bootstrapping. Stacking increases the SNR, in particular for faint galaxies, where the uncertainty in the mass is driven by the SNR in IRAC (see ?).

We derive stellar masses and redshifts by fitting stellar populations synthesis models to the average SED fluxes using the χ^2 -fitting code FAST (Kriek et al. 2009). We adopt Bruzual & Charlot (2003, BC03) models with a Salpeter (1955) initial mass function (IMF) between $0.1 - 100 M_{\odot}$. We explore several SFHs and the effects of metallicity and dust. The differences with more recent models (e.g., Maraston 2005, Charlot & Bruzual, in preparation) are small and will not be considered in detail (see Labbé et al. 2010). We fit models smoothed to a resolution of 100 \AA rest-frame, corresponding to

the approximate width of the dropout selection windows. Adopting a Kroupa (2001) IMF reduces the stellar masses and SFRs by 0.2 dex, but does not change other parameters or the quality of fit. The typical uncertainties in the derived average stellar masses, SFRs, age, and A_V for the stacked SEDs are 0.15 dex, 0.25 dex, 0.3 dex, and 0.1 mag, respectively. The photometry and best-fit model parameters are presented in Table 1.

3. STELLAR POPULATIONS AND STAR FORMATION HISTORIES AT $Z \sim 7$

Figure 1 (*left panel*) shows the broadband SEDs of the $z \sim 7$ z_{850} -dropout galaxies in the three magnitude bins, with the best-fit BC03 stellar population models. The overall SED shapes are remarkably similar, with a pronounced jump between H_{160} and $[3.6]$ (or rest-frame $(U - V) \approx 0.5$) indicative of a modest Balmer break and evolved stellar populations (> 100 Myr). Focusing on the far- UV continuum, we find the slope $f_{\lambda} \propto \lambda^{\beta}$ (traced by the $J_{125} - H_{160}$ color) to be very blue, and decreasing from $\beta \sim -2$ at $H_{160} \sim 26$ to $\beta \sim -3.0$ at $H_{160} \sim 28$. As discussed by Bouwens et al. (2010b), such extremely blue slopes require low dust content $A_V < 0.1$, very low metallicities and/or very young ages. Small 0.04 mag changes in the WFC3/IR zeropoints (e.g., McLure et al. (2009)) would cause changes of $\beta \approx 0.17$, comparable to the random uncertainties. The red $H_{160} - [3.6]$ color, however, implies more evolved stellar populations (> 100 Myr), leaving the models seemingly unable to match the entire SED.

To explore the mismatch further we consider in more detail the effects on metallicity, SFH, and nebular emission. Fig. 1 (*right panel*) shows the $J_{125} - H_{160}$ versus $H_{160} - [3.6]$ colors of the observed stacked SEDs. The lines show predictions of $0.2 Z_{\odot}$ BC03 models for various continuous SFHs (rising, constant, declining). Generally, evolved models are able to reproduce the joint $J_{125} - H_{160}$ versus $H_{160} - [3.6]$ colors of the more luminous $z = 7$ galaxies, but not the colors of the faintest, bluest galaxies. The arrows show the effect of changes in model assumptions, which we will discuss now:

1) *Metallicities*: Low metallicities (e.g., $0.2 Z_{\odot}$) do a decent job of producing much bluer β than Solar at a given $H_{160} - [3.6]$ color. Very low metallicities ($1/50$ Solar) produce even bluer β 's, but also bluer $H_{160} - [3.6]$. Metallicity alone appears not enough to fully resolve the discrepancy.

2) *Nebular Emission*: Nebular emission lines (NEL) likely contribute to the IRAC fluxes, reddening the $H_{160} - [3.6]$ color. Empirical estimates of $[\text{OIII}]\lambda 5007$ emission at $z > 2$ are scarce, but we can infer the possible effect from the observed strength of $H\alpha$ at $z \sim 2.2$ (Erb et al. 2006). Assuming $W_{H\alpha} = 200 \text{ \AA}$ and $W_{[\text{OIII}]\lambda 4959, 5007 + H\beta} = 2.5 \times W_{H\alpha}$, appropriate for $0.2 Z_{\odot}$ galaxies at $z > 2$ (Erb et al. 2006; Brinchmann et al. 2008), and adopting a redshift distribution of $z = 6.9 \pm 0.5$ (Oesch et al. 2010) we calculate a contribution of 0.18 mag to $[3.6]$ and 0.14 mag to $[4.5]$ (see Fig 1). Note however, that no measurements of nebular lines at $z \sim 7$ exist. A second possible effect is nebular continuum emission (NEC), which would cause a reddening of both β and $H_{160} - [3.6]$ (shown are the models of Schaerer 2002 with $Z = 1/50 Z_{\odot}$, $t = 300$ Myr CSF, and 0% escape fraction). Both would reduce the discrepancy between

¹¹ This paper uses data release DR2 of epoch 2, available from <http://data.spitzer.caltech.edu/popular/goods/>

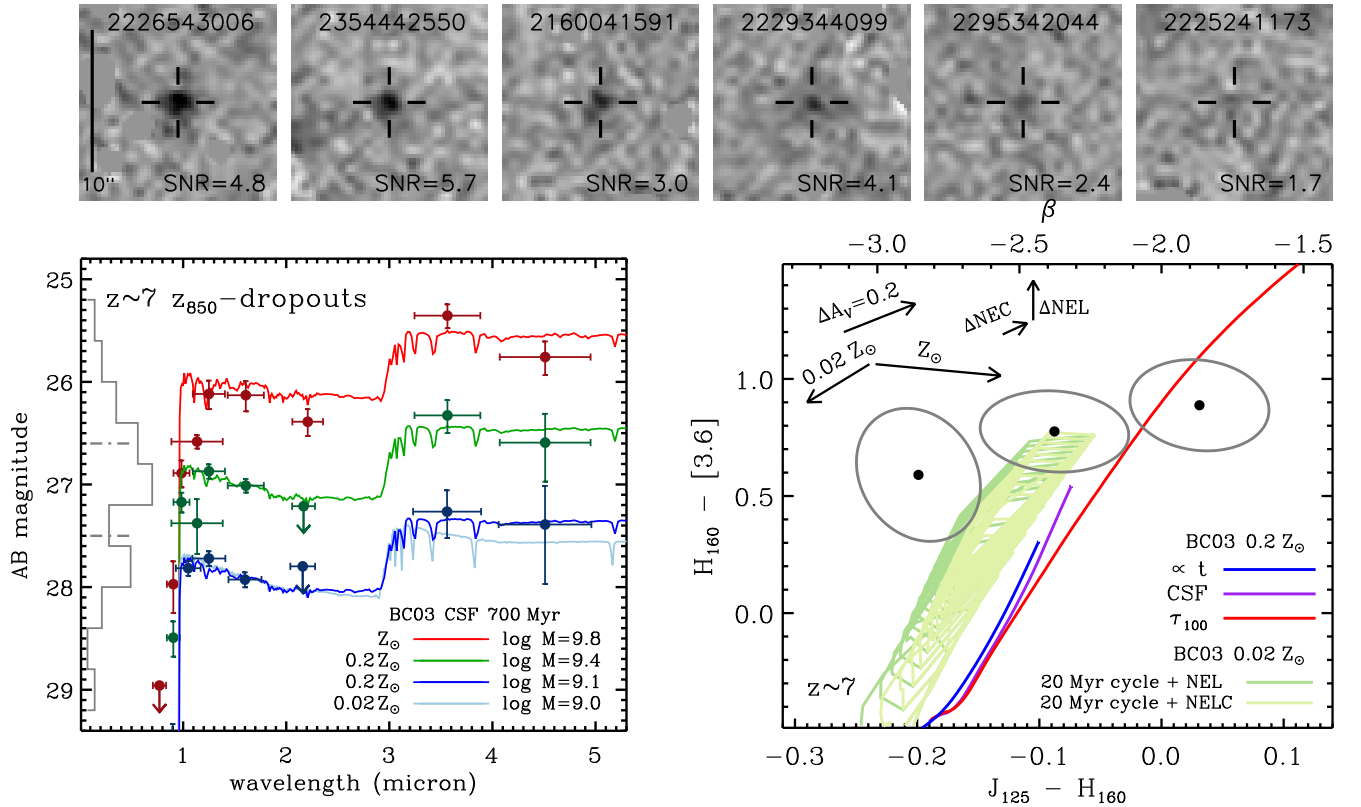


FIG. 1.— (*Top panels*) Representative IRAC [3.6] image stamps of WFC3/ERS $z \sim 7$ z_{850} -dropouts (sorted by magnitude) after subtracting neighbors. Brighter sources may have lower SNR after accounting for confusion. (*left panel*) Stacked broadband SEDs from the combined NICMOS, WFC3/UDF and WFC3/ERS samples, averaged in ~ 1 -mag bins centered on $H_{160} \approx 26, 27$ and 28 . The data include HST/ACS, NICMOS, and WFC3/IR, groundbased K , and IRAC [3.6] and [4.5]. Upper limits are 2σ . The gray histogram shows the H_{160} -band magnitude distribution (the peak is 9 sources). The best-fit BC03 stellar population models at $z = 6.9$ are shown. The overall SED shapes are similar with a break between H_{160} and [3.6], expected for evolved stellar populations (> 100 Myr). The far- UV slope (traced by $J_{125} - H_{160}$) bluels towards fainter H_{160} magnitude (as found Bouwens et al. 2010b). (*right panel*) Comparison of the observed average $J_{125} - H_{160}$ versus $H_{160} - [3.6]$ color (filled circles) with predictions of $0.2 Z_{\odot}$ BC03 models for various SFHs (solid lines). Ellipsoids show 1σ uncertainties. The SFHs are linearly increasing with time (blue), CSF (purple), episodic (light green) with a 50% duty cycle and 40Myr duration, and exponentially declining (red) with $\tau = 100$ Myr. Also shown are the effects on the model colors of metallicity, reddening (Calzetti et al. 2000), nebular continuum emission (NEC) (Schaerer 2002), and line emission (NEL) (Erb et al. 2006; Brinchmann et al. 2008). The episodic model is shown twice, once only with the effect of line emission (+ NEL) and once with both line and nebular continuum emission (+ NELC). The lines terminate at the 750Myr.

models and data by allowing the models to extend to redder $H_{160} - [3.6]$ at a given β . Note that the extremely blue β may require high escape fractions $f_{esc} \gtrsim 0.3$ (e.g., Bouwens et al. 2010b), which would reduce the contribution of nebular emission.

3) *Star Formation Histories*: Declining SFHs can match the colors of the most luminous, redder galaxies, but their far- UV continua are too red for lower luminosity galaxies. In contrast, strongly rising SFRs ($SFR \propto t^{\alpha}$, $\alpha > 1$) exhibit blue β but never reach red $H_{160} - [3.6]$ in a Hubble time ($z = 7$) and are formally excluded at 95% confidence. CSF is a compromise, providing red $H_{160} - [3.6]$ colors generated by on-going assembly of stellar mass, and blue far- UV continua from on-going star formation. Finally, episodic SFH with a 50% duty cycle and 40 Myr duration (i.e., 20 Myr “on”, 20 Myr “off”) are found to have an interesting mix of properties. The luminous active phase of the cycle produces a bluer far- UV continuum for a given $H_{160} - [3.6]$ color than CSF. The reverse is true in the dimmer passive state. The net result for a steep UV LF function is that the

luminosity weighted average of cycling galaxies displays bluer far- UV at a given $H_{160} - [3.6]$ than CSF, also reducing the discrepancy.

In summary, the model colors match the observations of luminous $z \sim 7$ galaxies reasonably except for the lowest luminosity galaxies, where the blue $\beta \sim -3$ and the red $H_{160} - [3.6] \sim 0.6$ colors remain challenging to fit. Low metallicity CSF models come close, but a contribution from nebular line emission to the [3.6]-band and/or episodic SFHs are likely needed to resolve the mismatch.

4. STAR FORMATION RATE VERSUS STELLAR MASS AT $Z \sim 7$

Independent constraints on the SFHs can be obtained from the relation between SFR and stellar mass, as shown in Fig. 2. The SFRs are calculated from the monochromatic 1500\AA luminosity following the prescription of Madau et al. (1998) and corrected for dust using the best-fit A_V . The galaxies are grouped in bins of SFR (or M_{1500}) centered on $\log SFR \approx 0.4, 0.8, 1.2$.

The stellar mass of our $z \sim 7$ sample correlates strongly with the SFR, producing $\log M^* = 8.70(\pm 0.09) +$

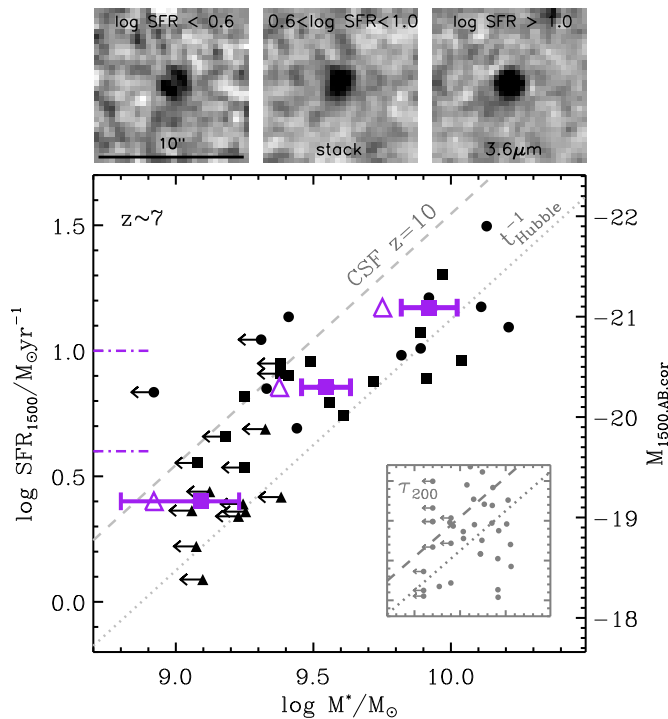


FIG. 2.— Average UV -derived, dust-corrected SFR versus stellar mass for $z \sim 7$ galaxies. Black symbols denote galaxies from the NICMOS (*circles*), WFC3/IR ERS (*squares*) and WFC3/IR HUDF sample (*triangles*). The purple squares show the average stellar mass in bins of SFR centered on $\log SFR \approx 0.4, 0.8, 1.2$. The purple triangles assume ≈ 0.2 and 0.15 mag contribution by emission lines to the $[3.6]$ and $[4.5]$ bands. The scatter in M^* in bins of M_{1500} is ~ 0.3 dex. The diagonal lines show the maximum stellar mass CSF stellar population can form in a Hubble time (*dotted*) or since $z = 10$ (*dashed*). Galaxies with strongly increasing/declining SFRs would lie well above/below the lines, respectively, but few such systems are found. The inset shows simulated galaxies with random formation times and exponentially declining $\tau = 200$ Myr SFHs, showing a different distribution with larger scatter. (*Top panels*) Stacked images in the $[3.6]$ band in bins of SFR.

$1.06(\pm 0.10) \log SFR$ and corresponding to a constant $M/L_V \approx 0.20$.¹² The derived stellar mass with emission lines (see §3) would be lower by ≈ 0.17 dex. The scatter around the relation is fairly low ≈ 0.3 dex, but that does not exclude significant short-term SFR variation, e.g., the episodic model (§3) predicts $\log M^* = 8.45 + 1.0 \log SFR_{1500}$ and a scatter of ~ 0.3 dex. We find no galaxies with SFRs much lower or higher than the past averaged SFR (i.e., strongly bursting or suppressed). Such galaxies would have satisfied our dropout criteria and would lie in the upper left or lower right corner in Fig. 2. Their absence suggests that the typical star formation timescales are probably a substantial fraction of the Hubble time. Instead we find that only 4/22 sources with $\log SFR > 0.7$ are undetected at $[3.6]$ and no galaxies in the sample have SFRs substantially less than M^*/t_{Hubble} .

To illustrate the diagnostic power of the $M^* - SFR$

¹² The M/L also be calculated from the individual galaxies, yielding the same answer (Gonzalez et al. 2009).

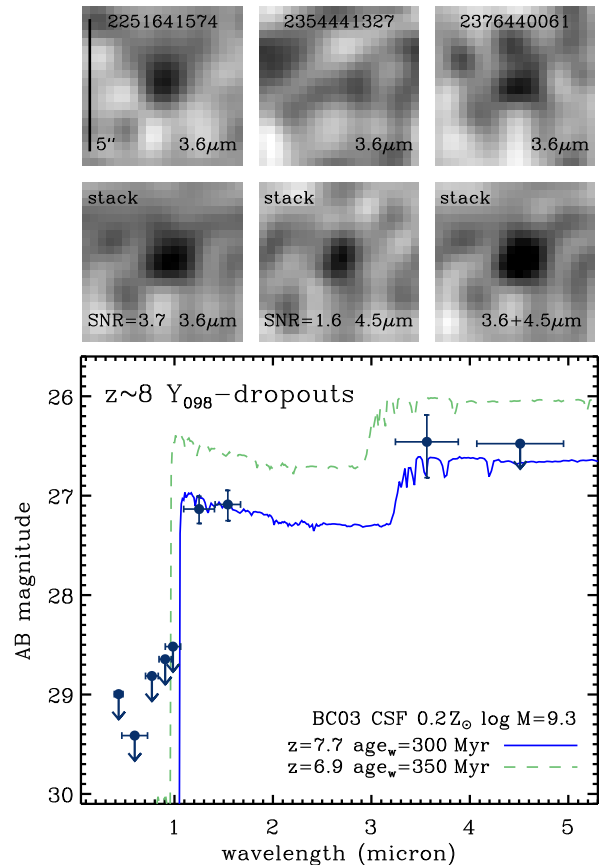


FIG. 3.— (*top panels*) Individual and stacked images of the 3 $z \sim 8$ Y_{098} -dropout galaxies in our WFC3/ERS sample, shown in inverted grayscale. Two of the 3 sources are individually detected in the IRAC $[3.6]$ -band. (*bottom panel*) The average broadband SED of the 3 $z \sim 8$ galaxies and the best-fit stellar population model (solid blue line). For comparison, we show the best-fit model to $z = 6.9$ z_{850} dropouts of similar H_{160} magnitude (dashed green line), shifted by -0.5 mag. The overall shapes are similar, with the $z \sim 8$ galaxies being slightly bluer in $H_{160} - [3.6]$ compared to $z \sim 7$ galaxies. Upper limits are 2σ .

diagram, we show in the inset in Fig. 2 a simulation of galaxies with random formation times and exponentially declining SFRs ($\tau = 200$ Myr) to the same selection limits as our observed sample. The distribution is clearly different, with no correlation between M^* and SFR, suggesting that star formation timescales for $z \sim 7$ galaxies are probably longer than that.

5. THE STELLAR MASS DENSITY AT $Z \sim 8$

The detection of $z \sim 8$ galaxies with IRAC is enticing as it enables us to place stronger constraints on the stellar masses of the highest redshift galaxies than possible from the far- UV alone. Recent studies in the HUDF have found no detection (individual or stacked) for $z \sim 8$ galaxy candidates (Labbé et al. 2010), leaving estimates of the stellar mass density at these redshifts highly uncertain.

Here we perform photometry on the 3 $z \sim 8$ Y_{098} -dropout galaxies in the WFC3/ERS sample of R. J. Bouwens et al. (in preparation). These candidates are

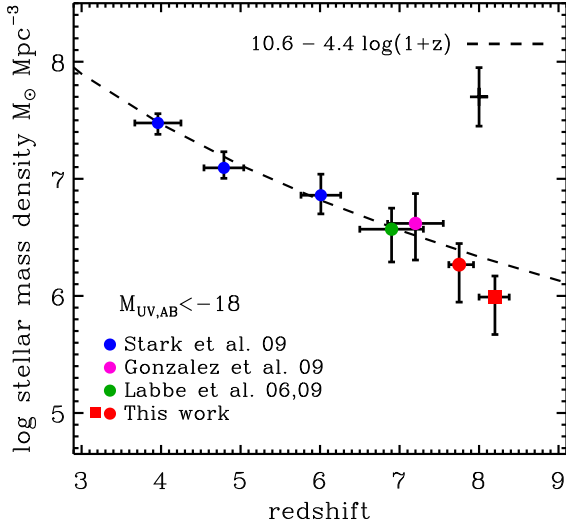


FIG. 4.— The evolution of the integrated stellar mass density. The red circle shows the $z \approx 7.7$ mass density, derived from the integrated UV -luminosity density of (Bouwens et al., in preparation) and the mean M/L derived here. All data are converted to a common limit $M_{UV,AB} < -18$, using the UV LFs of Bouwens et al. (2010a). The WFC3/ERS data are corrected by +0.42 dex. The $z = 3 - 7$ luminous samples ($M_{UV,AB} < -20$) from the literature (Stark et al. 2009 *blue circles*, Gonzalez et al. (2009), *magenta circle*) are corrected by +0.38, +0.46, +0.57, and +0.75 dex at $z=4, 5, 6$, and 7 , respectively. The HUDF requires no correction (Labbé et al. 2010, *green circle*). The red square shows the $z \approx 8.2$ sample of (Bouwens et al. 2010a), but using the M/L derived here for the $z \approx 7.7$ sources. The dashed line shows a $\propto (1+z)^{-4.4}$ evolution. The floating error bar indicates the expected cosmic variance for the $z \sim 8$ sample.

brighter than found in the HUDF ($H \approx 27$ versus $H \approx 28$). Two galaxies are detected at $[3.6]^{13}$ and we calculate an average $SNR = 3.7$ in $[3.6]$ and $SNR = 1.6$ in $[4.5]$ for the stack of all three (see Fig 3, top panels). The best fits are $z = 7.7^{+0.18}_{-0.15}$, high stellar age $age_w = 300^{+50}_{-210}$ Myr¹⁴, mass-to-light ratios $M/L_V = 0.15$ and $M/L_{1500} = 0.1$, and $\log SSFR = -8.7$. Overall these properties are comparable to $H \approx 27$ $z \sim 7$ z_{850} -dropouts, suggesting modest evolution in the M/L between $z = 8$ and $z = 7$.

Following the approach of Gonzalez et al. (2009) and Labbé et al. (2010), we derive integrated stellar mass densities at $z \sim 8$ by multiplying the UV -luminosity densities integrated to $M_{UV,AB} = -18$ (Bouwens et al. 2010a, R. J. Bouwens et al. in preparation) by the mean M/L derived for the $z \sim 7.7$ galaxies, yielding $\rho^*(z = 8) = 1.8^{+0.7}_{-1.0} \times 10^6 M_\odot \text{ Mpc}^{-3}$. We also recompute the $z \sim 8$ stellar mass density of Labbé et al. (2010) using the same M/L . Figure 4 shows the evolution of the stellar mass density from $z = 3$ to $z = 8$. The evolution over $3 < z < 8$ is well approximated by $\log \rho^*(z) = 10.6(\pm 0.6) - 4.4(\pm 0.7) \log(1+z) [M_\odot \text{ Mpc}^{-3}]$ over $3 < z < 8$.

¹³ We caution that source ERSy-2376440061 at $[3.6]$ is close to pixels that are affected by “Muxbled”, which we subtracted using a 3rd order polynomial fit to the $20'' \times 20''$ background before performing photometry.

¹⁴ Following Labbé et al. (2006) we report SFH weighted age_w , where $age_w = t/2$ for CSF and t is the time elapsed since the start of star formation.

6. SUMMARY

Using a large sample of 36 z_{850} -dropout galaxies based on deep/wide-area WFC3/IR data from the Early Release Science, ultradeep data from the HUDF09, and wide-area NICMOS programs, we investigate the stellar population properties at extreme redshifts $z \gtrsim 7$. The main results are:

- The average rest-frame far- UV slope at $z \sim 7$ becomes bluer with decreasing luminosity, from $\beta \sim -2.0$ ($L_{z=3}^*$) to $\beta \sim -3.0$ ($0.1 L_{z=3}^*$), as reported by Bouwens et al. (2010b). The rest-frame $U - V$ becomes bluer as well, but is still moderately red $U - V \approx 0.3$ at $0.1 L_{z=3}^*$, apparently excluding extremely young ages < 100 Myr. If the ages inferred from the simple model fits are correct, galaxies started forming stars very early-on, perhaps as high as $z > 10$. The blue far- UV slope and red $U - V$ colors remain a challenge to fit, however, even for sub-solar metallicity models. Episodic SFHs with periods of activity and quiescence and/or a (~ 0.2 mag) contribution of emission lines to the $[3.6]$ -band may be required to resolve the mismatch.
- The derived stellar masses correlate with the SFRs at $z \sim 7$ according to $\log M^* = 8.70(\pm 0.09) + 1.06(\pm 0.10) \log SFR$, with relatively low scatter ~ 0.25 dex. Emission line contributions of ≈ 0.2 mag to both $[3.6]$ and $[4.5]$ would shift the relation by ≈ -0.2 dex in mass. The absence of galaxies with SFRs much lower or higher than the past averaged SFR (i.e., strongly bursting or suppressed) suggests that the typical star formation timescales are probably a substantial fraction of the Hubble time. Note that instantaneously quenched galaxies may fade too quickly to be selected as dropout galaxies.
- The first Spitzer/IRAC detection of $z = 8$ galaxies and their red average $H_{160} - [3.6] \approx 0.55$ suggest that luminous early galaxies may have substantial $M/L_V \approx 0.15$, similar to $z = 7$ galaxies. The derived stellar mass density then increases gradually with time following $\log \rho^*(z) = 10.6(\pm 0.6) - 4.4(\pm 0.7) \log(1+z) [M_\odot \text{ Mpc}^{-3}]$ over $3 < z < 8$.

Deeper IRAC data on $z > 7$ galaxies are needed to bolster these results. More nebular emission line measurements of $z > 2$ galaxies would help to understand the possible contribution to the broadband fluxes. Additional modeling of the distribution of SFR versus M^* is needed to decipher the SFHs of $z \sim 7$ galaxies. Larger samples would enable a more secure assessment of the mass density evolution beyond $z = 8$.

We are grateful to all those at NASA, STScI, JPL, SSC who have made Hubble and Spitzer the remarkable observatories that they are today. IL acknowledges support from NASA through Hubble Fellowship grant HF-01209.01-A awarded by the STScI, which is operated by the AURA, Inc., for NASA, under contract NAS 5-26555. PO acknowledges support from the

Swiss National Foundation (SNF). We acknowledge the support of NASA grant NAG5-7697 and NASA grant HST-GO-11563.

Facilities: Spitzer (IRAC), HST (WFC3/IR), Magellan (PANIC), VLT (ISAAC)

REFERENCES

- Bouwens, R. J., et al. 2004, *ApJ*, 616, L79 (B04)
- Bouwens, R. J., Illingworth, G. D., Blakeslee, J. P., & Franx, M. 2006, *ApJ*, 653, 53
- Bouwens, R. J., Illingworth, G. D., Franx, M., & Ford, H. 2008, *ApJ*, 686, 230
- Bouwens, R. J., et al. 2010, *ApJ*, 709, L133
- Bouwens, R. J., et al. 2010, *ApJ*, 708, L69
- Brinchmann, J., Pettini, M., & Charlot, S. 2008, *MNRAS*, 385, 769
- Bunker, A. J. et al. 2004, *MNRAS*, 355, 374
- Bunker, A., et al. 2009, submitted, arXiv:0909.2255
- Bruzual, G. & Charlot, S. 2003, *MNRAS*, 344, 1000 (BC03)
- Calzetti, D., et al. 2000, *ApJ*, 533, 682
- Castellano, M., et al. 2009, arXiv:0909.2853
- Davé, R. 2008, *MNRAS*, 385, 147
- Erb, D. K., Shapley, A. E., Pettini, M., Steidel, C. C., Reddy, N. A., & Adelberger, K. L. 2006, *ApJ*, 644, 813
- Eyles, L. P., et al. 2005, *MNRAS*, 364, 443
- Egami, E., et al. 2005, *ApJ*, 618, L5
- Fazio, G. G., et al. 2004, *ApJS*, 154, 10
- Finlator, K., Davé, R., & Oppenheimer, B. D. 2007, *MNRAS*, 376, 1861
- Gonzalez, V., Labbe, I., Bouwens, R. J., Illingworth, G., Franx, M., Kriek, M., & Brammer, G. B. 2009, *ApJ*, in press, arXiv:0909.3517
- Hickey, S., Bunker, A., Jarvis, M. J., Chiu, K., & Bonfield, D. 2009, arXiv:0909.4205
- Kriek, M., van Dokkum, P. G., Labbé, I., Franx, M., Illingworth, G. D., Marchesini, D., & Quadri, R. F. 2009, *ApJ*, 700, 221
- Kroupa, P. 2001, *MNRAS*, 322, 231
- Labbé, I., et al. 2005, *ApJ*, 624, L81
- Labbé, I., Bouwens, R., Illingworth, G. D., & Franx, M. 2006, *ApJ*, 649, L67
- Labbé, I., et al. 2010, *ApJ*, 708, L26
- de Santis, C., Grazian, A., Fontana, A., & Santini, P. 2007, *New Astronomy*, 12, 271
- Lehnert, M. D., & Bremer, M. 2003, *ApJ*, 593, 630
- Madau, P., Pozzetti, L., & Dickinson, M. 1998, *ApJ*, 498, 106
- Maraston, C. 2005, *MNRAS*, 362, 799
- McLure, R. J., Dunlop, J. S., Cirasuolo, M., Koekemoer, A. M., Sabbi, E., Stark, D. P., Targett, T. A., & Ellis, R. S. 2009, arXiv:0909.2437
- Oke, J. B., & Gunn, J. E. 1983, *ApJ*, 266, 713
- Oesch, P. A., et al. 2009a, *ApJ*, 690, 1350
- Oesch, P. A., et al. 2010, *ApJ*, 709, L16
- Ouchi, M., et al. 2009, *ApJ*, 706, 1136
- Salpeter, E. E. 1955, *ApJ*, 121, 161
- Schaerer, D. 2002, *A&A*, 382, 28
- Stark, D. P., Ellis, R. S., Richard, J., Kneib, J.-P., Smith, G. P., & Santos, M. R. 2007, *ApJ*, 663, 10
- Stark, D. P., Ellis, R. S., Bunker, A., Bundy, K., Targett, T., Benson, A., & Lacy, M. 2009, *ApJ*, 697, 1493
- Steidel, C. C., Adelberger, K. L., Giavalisco, M., Dickinson, M., & Pettini, M. 1999, *ApJ*, 519, 1
- Trenti, M., & Stiavelli, M. 2008, *ApJ*, 676, 767
- Yan, H., et al. 2004, *ApJ*, 616, 63
- Yan, H., & Windhorst, R. A. 2004, *ApJ*, 600, L1
- Yan, H., Dickinson, M., Giavalisco, M., Stern, D., Eisenhardt, P. R. M., & Ferguson, H. C. 2006, *ApJ*, 651, 24
- van Dokkum, P. G. 2008, *ApJ*, 674, 29
- Wilkins, S. M., Bunker, A. J., Ellis, R. S., Stark, D., Stanway, E. R., Chiu, K., Lorenzoni, S., & Jarvis, M. J. 2009, arXiv:0910.1098
- Wuyts, S., et al. 2007, *ApJ*, 655, 51
- Yan, H., Windhorst, R., Hathi, N., Cohen, S., Ryan, R., O'Connell, R., & McCarthy, P. 2009, arXiv:0910.0077

TABLE 1
SUMMARY OF PHOTOMETRY AND MODELING OF $z \sim 7 - 8$ DROPOUT GALAXIES

SEDs of $z \sim 7$ z_{850} -dropouts										
	B_{435}	V_{606}	i_{775}	z_{850}	Y	J_{125}	H_{160}	K	[3.6]	[4.5]
ERS-2056344288	4.0(7.1)	1.2(5.0)	6.8(8.6)	13.5(9)	40.9(11)	48.6(8)	61.3(10)	—(—)	223.1(51)	134.7(89)
ERS-2068244221	-1.6(6.9)	2.4(5.5)	4.6(9.4)	26.4(10)	80.5(11)	78.3(15)	56.4(10)	—(—)	158.8(51)	-5.5(89)
ERS-2111644168	6.8(6.2)	1.5(4.7)	7.4(7.5)	4.9(8)	20.1(8)	54.8(10)	43.1(8)	—(—)	142.8(83)	-54.0(89)
ERS-2150242362	6.1(8.5)	0.9(7.5)	-3.5(12.5)	14.3(15)	33.4(15)	49.0(10)	68.7(14)	—(—)	154.4(58)	98.9(106)
ERS-2150943417	5.2(6.7)	4.7(6.0)	4.4(9.9)	9.2(12)	34.4(16)	87.7(17)	79.7(15)	—(—)	132.4(63)	197.3(120)
ERS-2154043286	-0.1(5.0)	-1.4(4.3)	4.8(7.4)	17.7(8)	45.3(9)	45.0(11)	36.5(9)	—(—)	11.5(62)	-13.5(100)
ERS-2160041591	-6.0(9.9)	-12.8(7.9)	4.7(13.5)	24.2(16)	68.2(15)	89.8(16)	74.7(14)	—(—)	271.0(87)	293.9(134)
ERS-2161941498	-0.8(7.1)	-1.4(5.7)	-3.2(9.8)	8.4(12)	25.7(10)	42.9(10)	41.6(10)	—(—)	64.4(51)	83.2(89)
ERS-2202443342	7.2(8.8)	-3.0(7.2)	5.6(10.3)	25.4(11)	42.5(11)	55.2(12)	50.4(11)	—(—)	145.9(51)	111.1(89)
ERS-2225241173	1.8(5.6)	-2.0(4.4)	-11.2(7.6)	15.3(8)	37.7(9)	40.6(8)	43.1(8)	—(—)	89.0(51)	128.2(89)
ERS-2226543006	-2.5(9.8)	-8.7(7.6)	7.8(12.5)	48.6(14)	113.3(15)	125.1(9)	182.5(13)	—(—)	462.9(94)	276.5(152)
ERS-2229344099	-0.6(8.3)	-0.6(7.0)	6.2(10.3)	18.8(11)	49.8(13)	47.0(8)	64.4(11)	—(—)	216.3(51)	110.8(89)
ERS-2295342044	-0.2(7.8)	1.4(5.7)	3.7(10.2)	14.5(12)	54.8(13)	70.9(13)	67.1(12)	—(—)	124.7(51)	82.3(89)
ERS-2352941047	-3.7(6.0)	4.1(4.6)	4.9(7.6)	8.6(9)	19.7(7)	28.9(6)	31.9(7)	—(—)	34.4(51)	54.4(89)
ERS-2354442550	3.7(6.2)	-0.7(4.6)	0.7(7.9)	15.1(9)	46.7(12)	117.4(12)	106.5(11)	—(—)	317.6(53)	21.5(101)
$25 < H_{160} < 26.5$	-3.2(2.3)	2.8(2.3)	-7.4(4.7)	23.5(5.4)	63.7(7.7)	129.7(16)	128.2(17)	101(12)	262(28)	181(37)
$26.5 < H_{160} < 27.5$	-2.4(0.8)	-0.8(0.6)	2.2(1.8)	14.6(2.3)	49.1(4.3)	64.8(4.1)	57.0(3.4)	24.5(24)	107(16)	83.8(25)
$H_{160} > 27.5$	1.2(0.8)	0.4(0.5)	-0.1(0.7)	5.6(1.1)	27.2(1.8)	29.6(2.0)	24.5(1.6)	22.9(14)	45.1(9.5)	39.3(17)

SEDs of $z \sim 8$ Y_{098} -dropouts										
	B_{435}	V_{606}	i_{775}	z_{850}	Y_{098}	J_{125}	H_{160}	K	[3.6]	[4.5]
ERSy-2354441327	-2.5(6.1)	-2.3(4.7)	-1.4(7.6)	-8.3(9)	1.6(8)	40.7(8)	37.3(7)	—(—)	29.9(52)	61.7(89)
ERSy-2376440061	-4.7(8.3)	2.6(5.5)	0.8(10.6)	15.0(11)	6.2(13)	46.5(12)	49.2(13)	—(—)	134.1(51)	143.6(89)
ERSy-2251641574	0.4(9.4)	-3.5(6.0)	2.1(9.9)	9.3(11)	5.9(14)	59.3(11)	69.6(13)	—(—)	103.1(51)	38.9(89)
$H_{160} \sim 27$	-1.9(4.6)	-1.3(3.1)	0.9(5.4)	6.9(6)	5.0(7)	50.8(6)	55.5(6)	—(—)	95.4(26)	77.4(49)

Average colors of $z \sim 7$ z_{850} -dropouts				SFRs and stellar masses of $z \sim 7$ z_{850} -dropouts			
	H_{160}	$J_{125} - H_{160}$	$H_{160} - [3.6]$		SFR_{1500}	M^*	$SSFR$
	[AB mag]	[AB mag]	[AB mag]		$[M_{\odot} \text{ yr}^{-1}]$	$[M_{\odot}]$	$[\text{yr}^{-1}]$
$25 < H_{160} < 26.6$	26.13(0.14)	0.03(0.06)	0.89(0.19)	$\log SFR > 1.0$	$1.17^{+0.05}_{-0.04}$	$9.92^{+0.06}_{-0.11}$	$-8.75^{+0.14}_{-0.08}$
$26.6 < H_{160} < 27.5$	26.98(0.05)	-0.09(0.06)	0.78(0.17)	$1.0 < \log SFR < 0.6$	$0.85^{+0.02}_{-0.02}$	$9.55^{+0.08}_{-0.07}$	$-8.70^{+0.12}_{-0.09}$
$H_{160} > 27.5$	27.92(0.10)	-0.20(0.05)	0.59(0.28)	$\log SFR < 0.6$	$0.39^{+0.05}_{-0.07}$	$9.08^{+0.12}_{-0.30}$	$-8.70^{+0.11}_{-0.07}$

NOTE. — The optical-to-near-IR fluxes are measured in $0''.4$ diameter apertures. Spitzer/IRAC fluxes are measured on the confusion-corrected maps in $2''.5$ diameter apertures. Fluxes are corrected to total assuming point source profiles. Units are nanoJy for the SEDs and AB magnitudes for the average colors. The total sample consists of 15 new sources from the WFC3/ERS sample (Bouwens et al., in preparation), 9 sources from the NICMOS sample (UDF-1417,964,GNS-1,2,3,4,5,CDFS-4627,HDFN-1216; Gonzalez et al. 2010), and 12 from the WFC3/UDF sample (UDFz-4471,4257,3955, 3958,3722,4314,3677,3744,4056,3638,3973,3853; Oesch et al. 2010, Labbé et al. 2010). The stacked Y -band of the $z \sim 7$ galaxies is a combination of the Y_{105} and Y_{098} bands. SFR_{1500} is the SFR derived from the 1500\AA monochromatic luminosity using the prescription of Madau et al. (1998) and corrected for dust using the best-fit A_V (mean $\langle A_V \rangle = 0.13$ mag). The stellar masses are based on BC03 $0.2Z_{\odot}$ models using exponentially declining SFHs with $8 < \log \tau < 11$ and reddening $A_V < 0.3$. Uncertainties are determined by bootstrapping.